Stem Cell Reports, Volume *16*

Supplemental Information

Novel Lineage-Tracing System to Identify Site-Specific Ectopic Bone Precursor Cells

Chase A. Pagani, Amanda K. Huber, Charles Hwang, Simone Marini, Karthik Padmanabhan, Nicholas Livingston, Johanna Nunez, Yuxiao Sun, Nicole Edwards, Yu-Hao Cheng, Noelle Visser, Pauline Yu, Nicole Patel, Joseph A. Greenstein, Husain Rasheed, Reagan Nelson, Karen Kessel, Kaetlin Vasquez, Amy L. Strong, Geoffrey E. Hespe, Jane Y. Song, Deneen M. Wellik, and Benjamin Levi

Figure S1

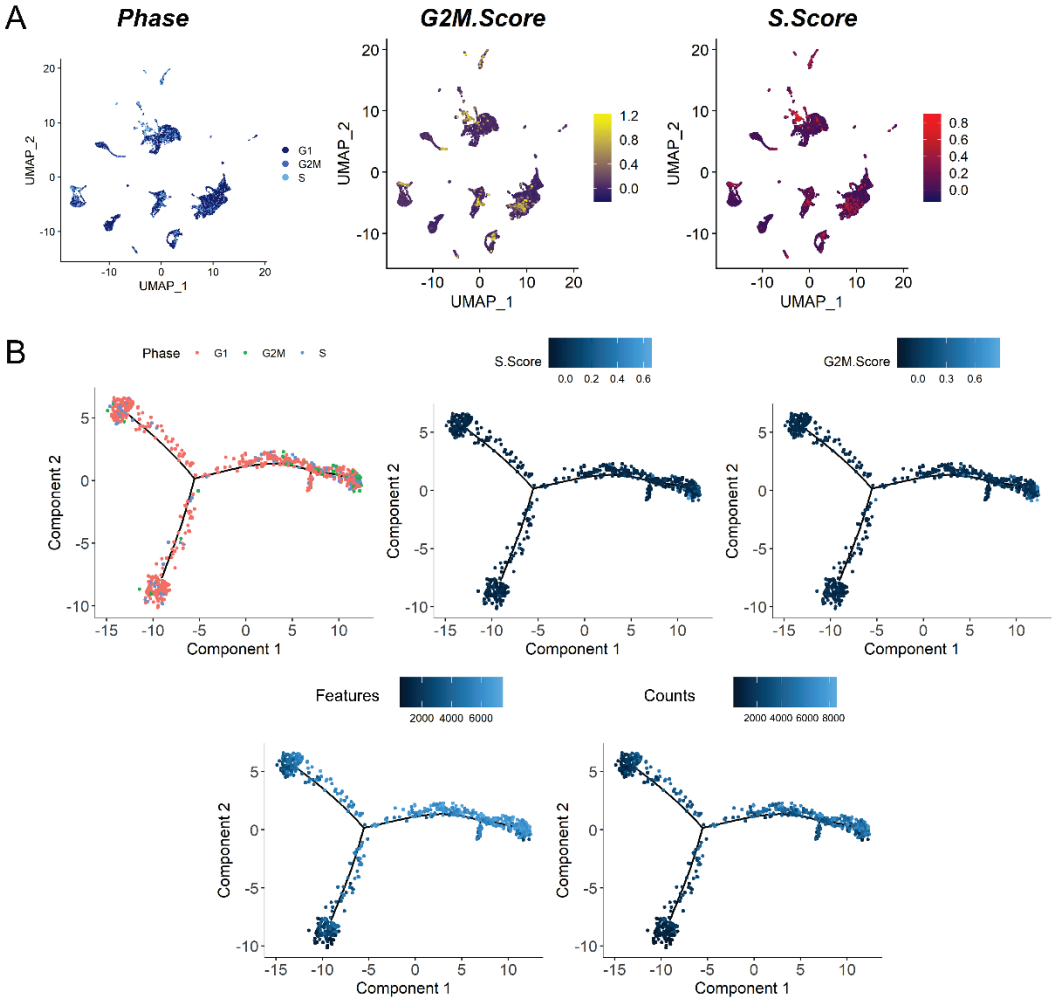

Figure S1. Single-Cell RNA sequencing cell cycle phase visualized on A) UMAP plots and B) trajectory analyses (top). Feature and counts also visualized on trajectories (bottom).

Figure S2

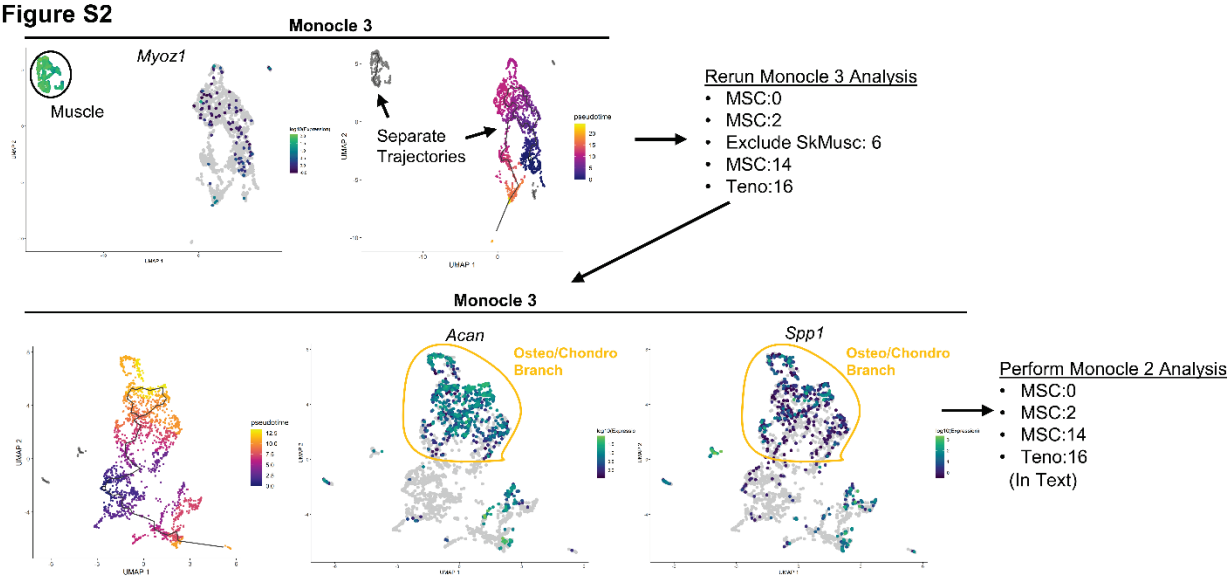

Figure S2. Single-Cell RNA-Sequencing Monocle 3 trajectory analysis. SkMusc:6 cluster did not share the same trajectory as other MSC populations. Monocle 3 was reperformed without SkMusc:6 to verify Osteo/Chondro branch was created by both Monocle 2 and 3.

Figure S3

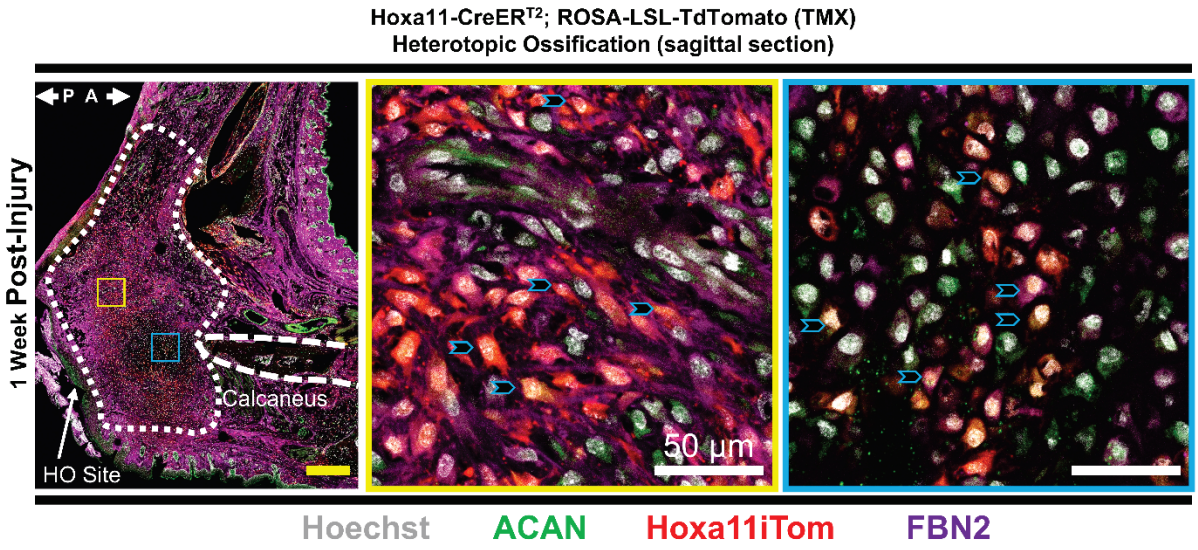

Figure S3. Confocal microscopy images of the hindlimb one-week following BT injury including tile scan image with dashed line marking calcaneus and dotted line marking HO (left) and 63x insets of region of interest. Sections were immunolabeled with indicated antibodies (bottom). Blue chevrons mark Hoxa11iTom cells co-labeled with specified antibodies. Yellow scale bars are 500 µm and white scale bars are 50 µm.

Figure S4

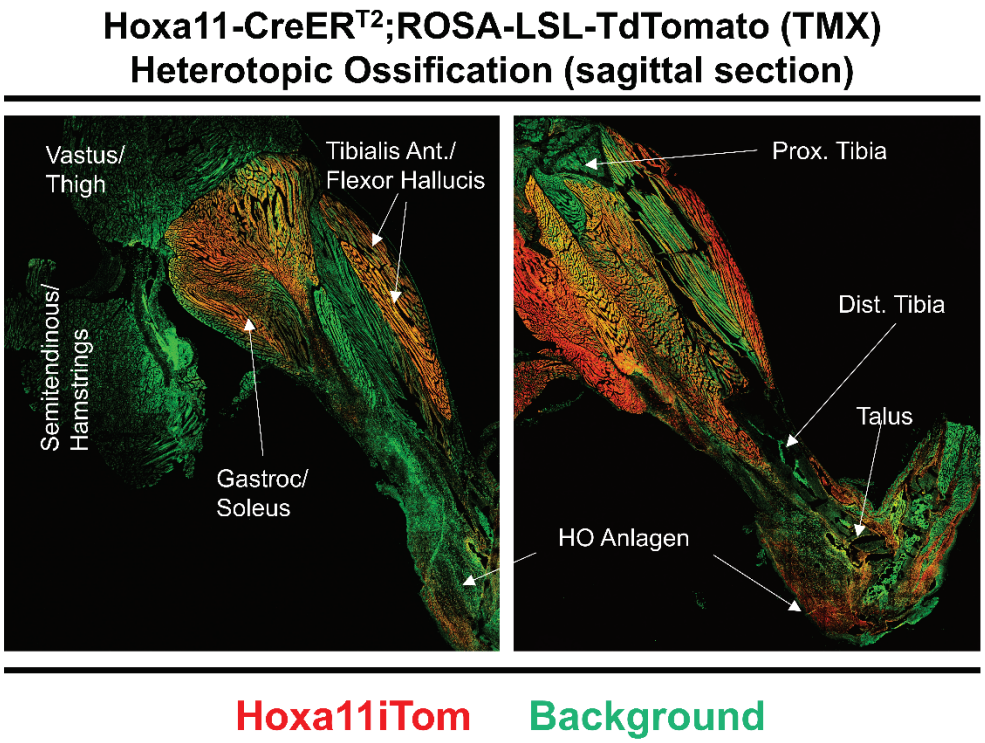

Figure S4. Confocal microscopy imaging shows that Hoxa11 TdTomato expression is limited to the limb zeugopod following burn/tenotomy injury and is not expressed in the upper mouse leg in two mouse samples (left and right). Background fluorescence (green), is shown for reference.

Figure S5

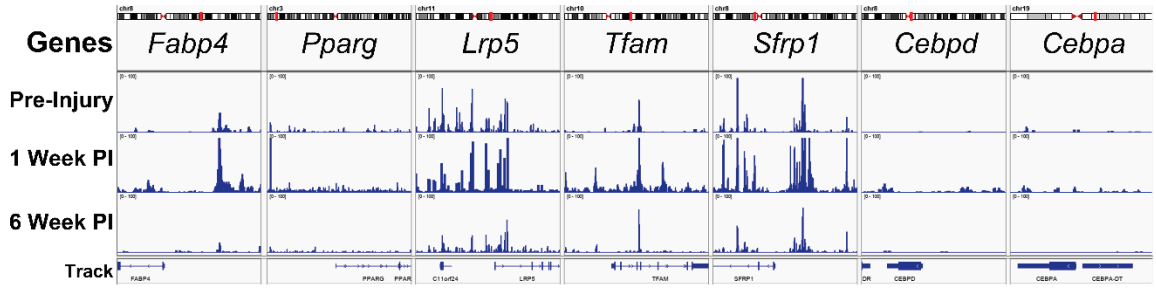

Figure S5. Single-nucleus ATAC sequencing of Hoxa11-lineage MSC cluster 0 shows open chromatin regions of adipogenic genes. Peaks show mean open chromatin reads.

Supplemental Table 1: Cluster marker genes.

Cluster	Gene Markers
MSC: 0	*Pdgfra*[1], *Acan*[2], *Fbn2*[3]
Macs: 1	*Mrc1*[4], *Csf1r*[5], *Adgre1*[6]
MSC: 2	*Pdgfra*[1], *Scara5*[7], *Clec3b*[8]
Endo: 3	*Pecam1*[9], *Mcam*[10]
Peri/SMC: 4	*Pdgfrb*[11], *Myh11*[12], *Abcc9*[13], *Pln*[14]
Kerat: 5	*Dmkn*[15], *Krt1*[16]
SkMusc: 6	*Des*[17], *Myoz1*[18]
PMN: 7	*Cxcr2*[19], *Camp*[20], *Mmp9*[21]
Gran: 8	*Ccr2*[22], *Il1b*[23]
B-Cell: 9	*Igkc*[24]
Skin Fblast: 10	*Krt15*[25], *Dmkn*[15]
DC: 11	*H2-Ab1*[26], *Il1b*[27], *Ccr2*[28]
NK: 12	*Il2rb*[29], *Cd2*[30]
Fblast: 13	*Col3a1*[31], *Sparc*[32], *Col1a1*[33], *Bgn*[34]
MSC: 14	*Pdgfra*[1], *Twist1*[35], *Pth1r*[36], *Wnt5a*[37]
LyEndo: 15	*Prox1*[38], *Flt4*[39]
Teno: 16	*Tnmd*[40], *Scx*[41], *Comp*[42]
Nerve: 17	*Sox10*[43], *Kcna1*[44], *Plp1*[45]
NK: 18	*Il2rb*[29], *Cd2*[30], *Cd7*[46]
P-DC: 19	*Cd7*[47], *Siglec*[48]
Mast: 20	*Cpa3*[49]
Satellite: 21	*Pax7*[50]
Stroma: 22	*Itgb4*[51], *Lepr*[52]
Oclast: 23	*Ocstamp*[53], *Mmp9*[54]
PMN: 24	*Fcnb*[55]

1. (Morikawa et al., 2009)
2. (Ono et al., 2014)
3. (Davis et al., 2014)
4. (Gordon and Martinez, 2010)
5. (Sherr et al., 1985)
6. (Waddell et al., 2018)
7. (Lee et al., 2017)
8. (Noack et al., 2014)
9. (Park et al., 2015)
10. (Wragg et al., 2016)
11. (Hou et al., 2018)
12. (Ray et al., 2020)
13. (Bondjers et al., 2006)
14. (Vanlandewijck et al., 2018)
15. (Matsui et al., 2004)
16. (Tao et al., 2007)
17. (Paulin and Li, 2004)
18. (Roberts et al., 2018)
19. (Sun et al., 2019)
20. (Herster et al., 2020)
21. (Wang et al., 2019b)
22. (Nywening et al., 2018)
23. (Drummond et al., 2019)
24. (Schmidt et al., 2012)
25. (Liu et al., 2003)
26. (Tesone et al., 2016)
27. (Mitsialis et al., 2020)
28. (Ruhland et al., 2020)
29. (Fernandez et al., 2019)
30. (Liu et al., 2016)
31. (Wang et al., 2019a)
32. (Drev et al., 2019)
33. (Li et al., 2020)
34. (Zhou et al., 2020)
35. (Fan et al., 2020)
36. (Cui et al., 2020)
37. (Diederichs et al., 2019)
38. (Wigle and Oliver, 1999)
39. (Karkkainen et al., 2004)
40. (Docheva et al., 2005)
41. (Huang et al., 2019)
42. (Smith et al., 1997)
43. (Fujiwara et al., 2014)
44. (Arroyo et al., 2001)
45. (Shy et al., 2003)
46. (Rabinowich et al., 1994)
47. (Zalmai et al., 2020)
48. (Perez-Zsolt et al., 2019)
49. (Lilla et al., 2011)
50. (Sambasivan et al., 2011)
51. (Bierie et al., 2017)
52. (Zhou et al., 2014)
53. (Yang et al., 2008)
54. (Sundaram et al., 2007)
55. (Tian et al., 2020)

Supplemental Table 2: Antibodies and dilutions used for immunofluorescent histology.

Antibody	Supplier and Catalogue #	Dilution (IF)
PDGFRα (goat)	R&D: AF1062	1:25
SOX9 (rabbit)	Abcam: ab185230	1:50
Phosphorylated SMAD3 (rabbit)	Novus: NBP1-77836	1:50
RUNX2 (rabbit)	Abcam: ab23981	1:50
Osteopontin (goat)	R&D: AF808	1:50
Osterix (rabbit)	Abcam: ab22552	1:50
Perilipin-1 (rabbit)	Cell Signaling: #9349	1:50
FBN2 (mouse)	Santa Cruz: sc-393968	1:50
ACAN (rabbit)	Abcam: ab36831	1:50
Alexa Fluor 488 (anti-goat)	Invitrogen: a21202	1:200
Alexa Fluor 647 (anti-goat)	Invitrogen: a21447	1:200
Alexa Fluor 647 (anti-rabbit)	Invitrogen: a31573	1:200
Hoechst 33342	Thermofisher: H3570	1:2000

SUPPLEMENTAL EXPERIMENTAL PROCEDURES

Tamoxifen Induction

Hoxa11-CreERT2;ROSA-TdTomato male and female mice six weeks of age were induced by feeding tamoxifen citrate chow (400mg/kg) for one week. Additionally, two intraperitoneal injections of tamoxifen (TMX; 75mg/kg) on days 0 and 2 were administered. Mice were allowed a washout period of four days before the BT injury.

BT Mouse Model

Mice were subjected to a BT injury as described previously [(Hwang et al., 2019); (Loder et al., 2018); (Sorkin et al., 2020)]. Briefly, mice were anesthetized and given buprenorphine analgesic prior to a complete transection of the left Achilles' tendon along with a dorsum burn of 30% total body surface area. The uninjured right leg served as an internal control.

Single Cell RNA Sequencing Preparation

scRNA and snATAC sequencing data are publicly available on GEO, GSE150995. Uninjured and post-surgery day 7 and 42 harvested tissue samples were processed as previously performed (Sorkin et al., 2020). Specifically, four mice were induced with tamoxifen as described in "Tamoxifen Induction" portion of experimental procedures. One mouse, serving as the uninjured control did not undergo the burn/tenotomy surgery. Three other mice underwent the burn/tenotomy injury. Cells from the uninjured control and from one of the injured mice were harvested seven days post-injury. Cells from the two remaining mice were harvested 42 days post-injury to ensure enough cells were harvested at the day 42 timepoint, as the inflammation and MSC proliferation at the injury site decreases significantly by day 42. Tissue was digested for 45 minutes in 750U/ml Type 1 Collagenase and 7U/ml Dispase II (Gibco) in Roswell Park Memorial Institute (RPMI) medium at 37°C under constant agitation at 180 rpm. Digestions were subsequently quenched with 2% FBS in PBS and filtered through 40µm sterile strainers. Cells were then washed in 2% FBS in PBS, counted and resuspended at a concentration of 1000-1200 cells/ul. Cell viability was assessed with Trypan blue exclusion on a Countess II (Thermo Fisher Scientific) automated counter and only samples with >85% viability were processed for further sequencing. For scRNA-seq we considered one replicate for day 0, one for day 7, and two replicates for day 42 and for snATAC-seq we considered one replicate each day 0, day 7, and day 42. Volumes corresponding to 5000 cell equivalents for scRNA-sequencing and 100,000 cell equivalents for snATAC-sequencing was removed for further processing. 5000 cells were processed for RNA libraries as described below. Before 10X library preparation, for snATAC-sequencing samples nuclei were extracted from 100,000 cells following the Nuclei Isolation for Single Cell ATAC Sequencing protocol (https://support.10xgenomics.com/single-cell-atac/sample-prep/doc/demonstrated-protocol-nuclei-isolation-for-single-cell-atac-sequencing) according to the manufacturer's guidelines. Library generation was performed using the 10x Genomics Chromium GEM Single Cell 3' Reagents kit v3.1 following the manufacturers protocol. Sequencing was performed on the Novaseq 6000 (Illumina, San Diego, CA, USA) S4 flowcell 300 cycle kit. This was loaded in order to target 500M reads/sample (5000 cells, 100K reads/cell), at 300pM (these were shared flowcells). The read length configuration was 150 x 8 x 150 cycles for Read 1, Index and Read 2, respectively. Cell Ranger Single Cell Software Suite 1.3 was used to perform sample de-multiplexing, barcode processing, and single cell gene counting (Alignment, Barcoding and UMI Count) at the University of Michigan Biomedical Core Facilities DNA Sequencing Core. For single ATAC sequencing, libraries were generated using the 10X Chromium Next GEM Single Cell ATAC kit v1.1; Chemistry with NextGEM Chip H. The sequencing was performed on the NovaSeq 6000 using the SP flowcell 100 cycle kit. Read lengths: 50 x 8 x 16 x 49.

Bioinformatics Analysis of Single Cell Sequencing Data

Seurat 3.1.1 (Butler et al., 2018) was used for downstream analysis. Cells with total expressed genes in the range of [500, 5000], [500, 6000], or [500, 7500], depending on the replicate, were retained. Cells with a fraction of mitochondrial gene UMIs higher than 0.25 were discarded. Filtered replicates were processed as Seurat objects. Seurat's FindVariableFeatures function was used with default parameters to determine highly variable genes, considering 2000 genes. Replicates were integrated according to the standard Seurat 3 workflow. Counts were normalized and variable genes were calculated (vst method) on each single replicate. The first 50 dimensions were considered for both finding integration anchors and integrate the replicates. The integrated set was then scaled, regressing out cell cycle gene scores and fraction of the mitochondrial gene UMIs. Unsupervised clustering was applied to the integrated set to find the cell communities (Louvain algorithm, resolution 0.35), leading to 25 clusters. The code to generate the Seurat object is available at https://github.com/smarini/Single-Cell-Downstream-analysis-Pagani-et-al.-2020. Markers for each cluster were calculated with FindMarkers using the negative binomial generalized linear model and ranked according to the difference in the fractions of cells expressing each marker

within cluster versus the rest of the considered cells. Clusters were labeled as cell type according to characteristic genes. After this, gene expression from all clusters were used to align the snATAC sequencing data using Signac 3.1.5 (https://github.com/timoast/signac). Briefly, snATAC data from the three conditions - day 0, day 7, and day 42 were merged after limiting the dataset to those cells that have at least 100 features. The resulting combined Seurat object was then normalized using default parameters and top variable features (peak accessibility) using a minimum cutoff of 20 cells were calculated. Dimension reduction was done using UMAP using dimensions 2 through 30 as input features. Unique clusters were determined using a shared nearest neighbor modularity optimization-based clustering algorithm with a resolution of 0.4. scRNA-seq data was used to guide the cluster labeling using `cca` reduction using the FindTransferAnchors function. This resulted in 9 cell-type based clusters in the snATAC data. Cells present in cluster 0 were extracted and bigWig files were generated for each condition (day 0, day 7 and day 42) using sinto (https://timoast.github.io/sinto/basic_usage.html#create-scatac-seq-fragments-file) and deeptools (Ramirez et al., 2016). Cells that had a least one count of *TdTomato* fluorophore transcript were included to create Figure 4E. Cells were characterized as *Sox9*, *Runx2,* or *Sox9 and Runx2* if they had at least one count of the respective gene transcript.

Cell Trajectories

Clusters 0, 2, 14, and 16 were used for cell trajectory analysis. Only cells with at least one count of *TdTomato* fluorophore transcript were included in the analysis. Cell trajectories were calculated with Monocle 2.13.0 (Trapnell et al., 2014), based on the top 2000 overall variable genes, ranked by scaled dispersion, obtained from Seurat. Further analysis using Monocle 3 0.2.3.0 confirmed that SkMusc:6 cluster formed a separate trajectory (Cao et al., 2019). The first 100 dimensions were considered. CytoTrace analysis were performed on the same cells through the internet application "Run Cytotrace" (https://cytotrace.stanford.edu/). The aligned bam files were subjected to Velocyto pipeline to obtain the counts of unspliced and spliced reads (La Manno et al., 2018). Cluster, cell features, and embedding information were extracted from the Seurat object in R and output to Python to integrate with the count matrix. The matrix was subsequently piped into the scVelo for RNA velocity estimation ((Bergen et al., 2020)). Genes were filtered by setting a minimal count threshold as 20 and a minimal unspliced count threshold as 10, and selected the top 2000 genes. The matrix was normalized and log-transformed. The first and second order moments for each cell were computed based on the top 30 principal components and the nearest 200 neighbors. RNA velocity was estimated by using the dynamical model and constructed the stream velocity graph. The latent time of each cell was calculated using the tl.latent_time function. The stream plot and latent time scatter plot were shown with cells embedded on top of the previously computed UMAP coordinates.

Immunofluorescence Histology and Confocal Microscopy

Mouse hind limb samples were harvested at one, three, and nine weeks after BT injury. The uninjured right leg served as an internal control and was harvested one week following left leg injury. Legs were fixed in 4% paraformaldehyde for 24 hours, washed with phosphate-buffered saline (PBS, Gibco, Waltham, MA), and then decalcified for 5 weeks in 17% EDTA (Sigma Aldrich, St. Louis, MO). Tissues were flash frozen in optimal cutting media for sectioning. Samples were oriented in blocks for sagittal sectioning. Tissue was cut into 7 µm sections and stored at -80°C. Sections were thawed, washed in 1X tris-buffered saline with tween-20 (TBST: 90% H_2O, 10% 10x tris-buffered saline (Bio-Rad, Hercules, CA), 0.05% tween-20, Sigma Aldrich, St. Louis, MO)) in preparation for immunofluorescence staining. Sections were blocked with donkey-serum block (10 ml solution: 0.1g BSA powder, 0.2 ml serum, 0.1 ml 10% cold water fish skin gelatin, 0.05 ml 20% TritonX-100, 0.05 ml 10% Tween-20, 3.0 ml 1M glycine, 1.0 ml 10x TBS pH 8.4, 5.6 ml Milli-Q water) for 2 hours at room temperature or Mouse-On-Mouse Blocking Kit (Vector Laboratories, Inc, Burlingame, CA) and stained with primary antibodies (**Supplemental Table 2**) diluted in antibody diluent (10 ml overnight at 4°C). Slides were then washed in TBST and incubated with secondary antibodies for 2 hours at room temperature. Slides were counter stained with Hoechst 33342 nuclear stain (Supplemental Table 1) for 5 minutes, washed in TBST, and mounted using ProLong Glass Antifade Mountant (Invitrogen, Carlsbad, CA) and #1.5 Slip-Rite cover glass (Richard-Allan Scientific, San Diego, California). Images were acquired using a Leica TCS SP8 microscope using the Leica LAS X software (Wetzlar, Germany). A White Light Laser with 20x objective (air) was used to capture full section tiled images, 20x magnification images, and 3.15x optical zoom images of regions of interest equivalent to 63x magnification.

Image Quantification

High resolution 20x lens, 3.15x zoom, images were counted by skilled operator for cell number quantification (*Hoxa11-CreER^{T2};ROSA-TdTomato* n=2 mice/antigen of interest, n=3 regions of interest/mouse). Hoechst 33342

stained channel nuclei were first counted to select whole cells within the image frame. Number of *Hoxa11*- lineage and antigen of interest expressing cells were counted for quantification. Mean and standard error was calculated, and graphs were created in GraphPad Prism 8 (GSL Biotech LLC, Chicago, IL).

Supplemental References

Arroyo, E.J., Xu, T., Poliak, S., Watson, M., Peles, E., and Scherer, S.S. (2001). Internodal specializations of myelinated axons in the central nervous system. Cell Tissue Res *305*, 53-66.

Bergen, V., Lange, M., Peidli, S., Wolf, F.A., and Theis, F.J. (2020). Generalizing RNA velocity to transient cell states through dynamical modeling. Nat Biotechnol *38*, 1408-1414.

Bierie, B., Pierce, S.E., Kroeger, C., Stover, D.G., Pattabiraman, D.R., Thiru, P., Liu Donaher, J., Reinhardt, F., Chaffer, C.L., Keckesova, Z.*, et al.* (2017). Integrin-beta4 identifies cancer stem cell-enriched populations of partially mesenchymal carcinoma cells. Proc Natl Acad Sci U S A *114*, E2337-E2346.

Bondjers, C., He, L., Takemoto, M., Norlin, J., Asker, N., Hellstrom, M., Lindahl, P., and Betsholtz, C. (2006). Microarray analysis of blood microvessels from PDGF-B and PDGF-Rbeta mutant mice identifies novel markers for brain pericytes. FASEB J *20*, 1703-1705.

Butler, A., Hoffman, P., Smibert, P., Papalexi, E., and Satija, R. (2018). Integrating single-cell transcriptomic data across different conditions, technologies, and species. Nat Biotechnol *36*, 411-420.

Cao, J., Spielmann, M., Qiu, X., Huang, X., Ibrahim, D.M., Hill, A.J., Zhang, F., Mundlos, S., Christiansen, L., Steemers, F.J.*, et al.* (2019). The single-cell transcriptional landscape of mammalian organogenesis. Nature *566*, 496-502.

Cui, C., Bi, R., Liu, W., Guan, S., Li, P., Song, D., Xu, R., Zheng, L., Yuan, Q., Zhou, X.*, et al.* (2020). Role of PTH1R Signaling in Prx1(+) Mesenchymal Progenitors during Eruption. J Dent Res *99*, 1296-1305.

Davis, M.R., Andersson, R., Severin, J., de Hoon, M., Bertin, N., Baillie, J.K., Kawaji, H., Sandelin, A., Forrest, A.R., Summers, K.M.*, et al.* (2014). Transcriptional profiling of the human fibrillin/LTBP gene family, key regulators of mesenchymal cell functions. Mol Genet Metab *112*, 73-83.

Diederichs, S., Tonnier, V., Marz, M., Dreher, S.I., Geisbusch, A., and Richter, W. (2019). Regulation of WNT5A and WNT11 during MSC in vitro chondrogenesis: WNT inhibition lowers BMP and hedgehog activity, and reduces hypertrophy. Cell Mol Life Sci *76*, 3875-3889.

Docheva, D., Hunziker, E.B., Fassler, R., and Brandau, O. (2005). Tenomodulin is necessary for tenocyte proliferation and tendon maturation. Mol Cell Biol *25*, 699-705.

Drev, D., Harpain, F., Beer, A., Stift, A., Gruber, E.S., Klimpfinger, M., Thalhammer, S., Reti, A., Kenner, L., Bergmann, M.*, et al.* (2019). Impact of Fibroblast-Derived SPARC on Invasiveness of Colorectal Cancer Cells. Cancers (Basel) *11*.

Drummond, R.A., Swamydas, M., Oikonomou, V., Zhai, B., Dambuza, I.M., Schaefer, B.C., Bohrer, A.C., Mayer-Barber, K.D., Lira, S.A., Iwakura, Y.*, et al.* (2019). CARD9(+) microglia promote antifungal immunity via IL-1beta- and CXCL1-mediated neutrophil recruitment. Nat Immunol *20*, 559-570.

Fan, X., Waardenberg, A.J., Demuth, M., Osteil, P., Sun, J.Q.J., Loebel, D.A.F., Graham, M., Tam, P.P.L., and Fossat, N. (2020). TWIST1 Homodimers and Heterodimers Orchestrate Lineage-Specific Differentiation. Mol Cell Biol *40*.

Fernandez, I.Z., Baxter, R.M., Garcia-Perez, J.E., Vendrame, E., Ranganath, T., Kong, D.S., Lundquist, K., Nguyen, T., Ogolla, S., Black, J.*, et al.* (2019). A novel human IL2RB mutation results in T and NK cell-driven immune dysregulation. J Exp Med *216*, 1255-1267.
Fujiwara, S., Hoshikawa, S., Ueno, T., Hirata, M., Saito, T., Ikeda, T., Kawaguchi, H., Nakamura, K., Tanaka, S., and Ogata, T. (2014). SOX10 transactivates S100B to suppress Schwann cell proliferation and to promote myelination. PLoS One *9*, e115400.
Gordon, S., and Martinez, F.O. (2010). Alternative activation of macrophages: mechanism and functions. Immunity *32*, 593-604.
Herster, F., Bittner, Z., Archer, N.K., Dickhofer, S., Eisel, D., Eigenbrod, T., Knorpp, T., Schneiderhan-Marra, N., Loffler, M.W., Kalbacher, H.*, et al.* (2020). Neutrophil extracellular trap-associated RNA and LL37 enable self-amplifying inflammation in psoriasis. Nat Commun *11*, 105.
Hou, Z., Wang, X., Cai, J., Zhang, J., Hassan, A., Auer, M., and Shi, X. (2018). Platelet-Derived Growth Factor Subunit B Signaling Promotes Pericyte Migration in Response to Loud Sound in the Cochlear Stria Vascularis. J Assoc Res Otolaryngol *19*, 363-379.
Huang, A.H., Watson, S.S., Wang, L., Baker, B.M., Akiyama, H., Brigande, J.V., and Schweitzer, R. (2019). Requirement for scleraxis in the recruitment of mesenchymal progenitors during embryonic tendon elongation. Development *146*.
Hwang, C., Marini, S., Huber, A.K., Stepien, D.M., Sorkin, M., Loder, S., Pagani, C.A., Li, J., Visser, N.D., Vasquez, K.*, et al.* (2019). Mesenchymal VEGFA induces aberrant differentiation in heterotopic ossification. Bone Res *7*, 36.
Karkkainen, M.J., Haiko, P., Sainio, K., Partanen, J., Taipale, J., Petrova, T.V., Jeltsch, M., Jackson, D.G., Talikka, M., Rauvala, H.*, et al.* (2004). Vascular endothelial growth factor C is required for sprouting of the first lymphatic vessels from embryonic veins. Nat Immunol *5*, 74-80.
La Manno, G., Soldatov, R., Zeisel, A., Braun, E., Hochgerner, H., Petukhov, V., Lidschreiber, K., Kastriti, M.E., Lonnerberg, P., Furlan, A.*, et al.* (2018). RNA velocity of single cells. Nature *560*, 494-498.
Lee, H., Lee, Y.J., Choi, H., Seok, J.W., Yoon, B.K., Kim, D., Han, J.Y., Lee, Y., Kim, H.J., and Kim, J.W. (2017). SCARA5 plays a critical role in the commitment of mesenchymal stem cells to adipogenesis. Sci Rep *7*, 14833.
Li, M., Wang, J., Wang, C., Xia, L., Xu, J., Xie, X., and Lu, W. (2020). Microenvironment remodeled by tumor and stromal cells elevates fibroblast-derived COL1A1 and facilitates ovarian cancer metastasis. Exp Cell Res *394*, 112153.
Lilla, J.N., Chen, C.C., Mukai, K., BenBarak, M.J., Franco, C.B., Kalesnikoff, J., Yu, M., Tsai, M., Piliponsky, A.M., and Galli, S.J. (2011). Reduced mast cell and basophil numbers and function in Cpa3-Cre; Mcl-1fl/fl mice. Blood *118*, 6930-6938.
Liu, L.L., Landskron, J., Ask, E.H., Enqvist, M., Sohlberg, E., Traherne, J.A., Hammer, Q., Goodridge, J.P., Larsson, S., Jayaraman, J.*, et al.* (2016). Critical Role of CD2 Co-stimulation in Adaptive Natural Killer Cell Responses Revealed in NKG2C-Deficient Humans. Cell Rep *15*, 1088-1099.
Liu, Y., Lyle, S., Yang, Z., and Cotsarelis, G. (2003). Keratin 15 promoter targets putative epithelial stem cells in the hair follicle bulge. J Invest Dermatol *121*, 963-968.
Loder, S.J., Agarwal, S., Chung, M.T., Cholok, D., Hwang, C., Visser, N., Vasquez, K., Sorkin, M., Habbouche, J., Sung, H.H.*, et al.* (2018). Characterizing the Circulating Cell Populations in Traumatic Heterotopic Ossification. Am J Pathol *188*, 2464-2473.

Matsui, T., Hayashi-Kisumi, F., Kinoshita, Y., Katahira, S., Morita, K., Miyachi, Y., Ono, Y., Imai, T., Tanigawa, Y., Komiya, T.*, et al.* (2004). Identification of novel keratinocyte-secreted peptides dermokine-alpha/-beta and a new stratified epithelium-secreted protein gene complex on human chromosome 19q13.1. Genomics *84*, 384-397.
Mitsialis, V., Wall, S., Liu, P., Ordovas-Montanes, J., Parmet, T., Vukovic, M., Spencer, D., Field, M., McCourt, C., Toothaker, J.*, et al.* (2020). Single-Cell Analyses of Colon and Blood Reveal Distinct Immune Cell Signatures of Ulcerative Colitis and Crohn's Disease. Gastroenterology *159*, 591-608 e510.
Morikawa, S., Mabuchi, Y., Kubota, Y., Nagai, Y., Niibe, K., Hiratsu, E., Suzuki, S., Miyauchi-Hara, C., Nagoshi, N., Sunabori, T.*, et al.* (2009). Prospective identification, isolation, and systemic transplantation of multipotent mesenchymal stem cells in murine bone marrow. J Exp Med *206*, 2483-2496.
Noack, S., Seiffart, V., Willbold, E., Laggies, S., Winkel, A., Shahab-Osterloh, S., Florkemeier, T., Hertwig, F., Steinhoff, C., Nuber, U.A.*, et al.* (2014). Periostin secreted by mesenchymal stem cells supports tendon formation in an ectopic mouse model. Stem Cells Dev *23*, 1844-1857.
Nywening, T.M., Belt, B.A., Cullinan, D.R., Panni, R.Z., Han, B.J., Sanford, D.E., Jacobs, R.C., Ye, J., Patel, A.A., Gillanders, W.E.*, et al.* (2018). Targeting both tumour-associated CXCR2(+) neutrophils and CCR2(+) macrophages disrupts myeloid recruitment and improves chemotherapeutic responses in pancreatic ductal adenocarcinoma. Gut *67*, 1112-1123.
Ono, N., Ono, W., Nagasawa, T., and Kronenberg, H.M. (2014). A subset of chondrogenic cells provides early mesenchymal progenitors in growing bones. Nat Cell Biol *16*, 1157-1167.
Park, S., Sorenson, C.M., and Sheibani, N. (2015). PECAM-1 isoforms, eNOS and endoglin axis in regulation of angiogenesis. Clin Sci (Lond) *129*, 217-234.
Paulin, D., and Li, Z. (2004). Desmin: a major intermediate filament protein essential for the structural integrity and function of muscle. Exp Cell Res *301*, 1-7.
Perez-Zsolt, D., Martinez-Picado, J., and Izquierdo-Useros, N. (2019). When Dendritic Cells Go Viral: The Role of Siglec-1 in Host Defense and Dissemination of Enveloped Viruses. Viruses *12*.
Rabinowich, H., Pricop, L., Herberman, R.B., and Whiteside, T.L. (1994). Expression and function of CD7 molecule on human natural killer cells. J Immunol *152*, 517-526.
Ramirez, F., Ryan, D.P., Gruning, B., Bhardwaj, V., Kilpert, F., Richter, A.S., Heyne, S., Dundar, F., and Manke, T. (2016). deepTools2: a next generation web server for deep-sequencing data analysis. Nucleic Acids Res *44*, W160-165.
Ray, H.C., Corliss, B.A., Bruce, A.C., Kesting, S., Dey, P., Mansour, J., Seaman, S.A., Smolko, C.M., Mathews, C., Dey, B.K.*, et al.* (2020). Myh11+ microvascular mural cells and derived mesenchymal stem cells promote retinal fibrosis. Sci Rep *10*, 15808.
Roberts, M.D., Romero, M.A., Mobley, C.B., Mumford, P.W., Roberson, P.A., Haun, C.T., Vann, C.G., Osburn, S.C., Holmes, H.H., Greer, R.A.*, et al.* (2018). Skeletal muscle mitochondrial volume and myozenin-1 protein differences exist between high versus low anabolic responders to resistance training. PeerJ *6*, e5338.
Ruhland, M.K., Roberts, E.W., Cai, E., Mujal, A.M., Marchuk, K., Beppler, C., Nam, D., Serwas, N.K., Binnewies, M., and Krummel, M.F. (2020). Visualizing Synaptic Transfer of Tumor Antigens among Dendritic Cells. Cancer Cell *37*, 786-799 e785.
Sambasivan, R., Yao, R., Kissenpfennig, A., Van Wittenberghe, L., Paldi, A., Gayraud-Morel, B., Guenou, H., Malissen, B., Tajbakhsh, S., and Galy, A. (2011). Pax7-expressing satellite cells are indispensable for adult skeletal muscle regeneration. Development *138*, 3647-3656.

Schmidt, M., Micke, P., Gehrmann, M., and Hengstler, J.G. (2012). Immunoglobulin kappa chain as an immunologic biomarker of prognosis and chemotherapy response in solid tumors. Oncoimmunology *1*, 1156-1158.
Sherr, C.J., Rettenmier, C.W., Sacca, R., Roussel, M.F., Look, A.T., and Stanley, E.R. (1985). The c-fms proto-oncogene product is related to the receptor for the mononuclear phagocyte growth factor, CSF-1. Cell *41*, 665-676.
Shy, M.E., Hobson, G., Jain, M., Boespflug-Tanguy, O., Garbern, J., Sperle, K., Li, W., Gow, A., Rodriguez, D., Bertini, E.*, et al.* (2003). Schwann cell expression of PLP1 but not DM20 is necessary to prevent neuropathy. Ann Neurol *53*, 354-365.
Smith, R.K., Zunino, L., Webbon, P.M., and Heinegard, D. (1997). The distribution of cartilage oligomeric matrix protein (COMP) in tendon and its variation with tendon site, age and load. Matrix Biol *16*, 255-271.
Sorkin, M., Huber, A.K., Hwang, C., Carson, W.F.t., Menon, R., Li, J., Vasquez, K., Pagani, C., Patel, N., Li, S.*, et al.* (2020). Regulation of heterotopic ossification by monocytes in a mouse model of aberrant wound healing. Nat Commun *11*, 722.
Sun, L., Clavijo, P.E., Robbins, Y., Patel, P., Friedman, J., Greene, S., Das, R., Silvin, C., Van Waes, C., Horn, L.A.*, et al.* (2019). Inhibiting myeloid-derived suppressor cell trafficking enhances T cell immunotherapy. JCI Insight *4*.
Sundaram, K., Nishimura, R., Senn, J., Youssef, R.F., London, S.D., and Reddy, S.V. (2007). RANK ligand signaling modulates the matrix metalloproteinase-9 gene expression during osteoclast differentiation. Exp Cell Res *313*, 168-178.
Tao, H., Berno, A.J., Cox, D.R., and Frazer, K.A. (2007). In vitro human keratinocyte migration rates are associated with SNPs in the KRT1 interval. PLoS One *2*, e697.
Tesone, A.J., Rutkowski, M.R., Brencicova, E., Svoronos, N., Perales-Puchalt, A., Stephen, T.L., Allegrezza, M.J., Payne, K.K., Nguyen, J.M., Wickramasinghe, J.*, et al.* (2016). Satb1 Overexpression Drives Tumor-Promoting Activities in Cancer-Associated Dendritic Cells. Cell Rep *14*, 1774-1786.
Tian, X., Zheng, Y., Yin, K., Ma, J., Tian, J., Zhang, Y., Mao, L., Xu, H., and Wang, S. (2020). LncRNA AK036396 Inhibits Maturation and Accelerates Immunosuppression of Polymorphonuclear Myeloid-Derived Suppressor Cells by Enhancing the Stability of Ficolin B. Cancer Immunol Res *8*, 565-577.
Trapnell, C., Cacchiarelli, D., Grimsby, J., Pokharel, P., Li, S., Morse, M., Lennon, N.J., Livak, K.J., Mikkelsen, T.S., and Rinn, J.L. (2014). The dynamics and regulators of cell fate decisions are revealed by pseudotemporal ordering of single cells. Nat Biotechnol *32*, 381-386.
Vanlandewijck, M., He, L., Mae, M.A., Andrae, J., Ando, K., Del Gaudio, F., Nahar, K., Lebouvier, T., Lavina, B., Gouveia, L.*, et al.* (2018). A molecular atlas of cell types and zonation in the brain vasculature. Nature *554*, 475-480.
Waddell, L.A., Lefevre, L., Bush, S.J., Raper, A., Young, R., Lisowski, Z.M., McCulloch, M.E.B., Muriuki, C., Sauter, K.A., Clark, E.L.*, et al.* (2018). ADGRE1 (EMR1, F4/80) Is a Rapidly-Evolving Gene Expressed in Mammalian Monocyte-Macrophages. Front Immunol *9*, 2246.
Wang, R., Zhang, M., Ou, Z., He, W., Chen, L., Zhang, J., He, Y., Xu, R., Jiang, S., Qi, L.*, et al.* (2019a). Long noncoding RNA DNM3OS promotes prostate stromal cells transformation via the miR-29a/29b/COL3A1 and miR-361/TGFbeta1 axes. Aging (Albany NY) *11*, 9442-9460.
Wang, X., Rojas-Quintero, J., Wilder, J., Tesfaigzi, Y., Zhang, D., and Owen, C.A. (2019b). Tissue Inhibitor of Metalloproteinase-1 Promotes Polymorphonuclear Neutrophil (PMN)

Pericellular Proteolysis by Anchoring Matrix Metalloproteinase-8 and -9 to PMN Surfaces. J Immunol *202*, 3267-3281.
Wigle, J.T., and Oliver, G. (1999). Prox1 function is required for the development of the murine lymphatic system. Cell *98*, 769-778.
Wragg, J.W., Finnity, J.P., Anderson, J.A., Ferguson, H.J., Porfiri, E., Bhatt, R.I., Murray, P.G., Heath, V.L., and Bicknell, R. (2016). MCAM and LAMA4 Are Highly Enriched in Tumor Blood Vessels of Renal Cell Carcinoma and Predict Patient Outcome. Cancer Res *76*, 2314-2326.
Yang, M., Birnbaum, M.J., MacKay, C.A., Mason-Savas, A., Thompson, B., and Odgren, P.R. (2008). Osteoclast stimulatory transmembrane protein (OC-STAMP), a novel protein induced by RANKL that promotes osteoclast differentiation. J Cell Physiol *215*, 497-505.
Zalmai, L., Viailly, P.J., Biichle, S., Cheok, M., Soret, L., Angelot-Delettre, F., Petrella, T., Collonge-Rame, M.A., Seilles, E., Geffroy, S.*, et al.* (2020). Plasmacytoid dendritic cells proliferation associated with acute myeloid leukemia: phenotype profile and mutation landscape. Haematologica *Online ahead of print*.
Zhou, B.O., Yue, R., Murphy, M.M., Peyer, J.G., and Morrison, S.J. (2014). Leptin-receptor-expressing mesenchymal stromal cells represent the main source of bone formed by adult bone marrow. Cell Stem Cell *15*, 154-168.
Zhou, Y., Bian, S., Zhou, X., Cui, Y., Wang, W., Wen, L., Guo, L., Fu, W., and Tang, F. (2020). Single-Cell Multiomics Sequencing Reveals Prevalent Genomic Alterations in Tumor Stromal Cells of Human Colorectal Cancer. Cancer Cell *38*, 818-828 e815.